Ordered Donor-Acceptor Complex Formation and Electron Transfer in Co-deposited Films of Structurally Dissimilar Molecules

Andreas Opitz, [a]* Clea Peter, [a] Berthold Wegner, [ab] H.S.S. Ramakrishna Matte, [a†] Adriana Röttger, [a] Timo Florian, [a] Xiaomin Xu, [a‡] Paul Beyer, [a§] Lutz Grubert, [c] Stefan Hecht, [c**] Valentina Belova, [d††] Alexander Hinderhofer, [d] Frank Schreiber, [d] Christian Kasper, [e] Jens Pflaum, [e] Yadong Zhang, [f] Stephen Barlow, [f] Seth R. Marder, [f] and Norbert Koch [ab]

a. Institut für Physik and IRIS Adlershof, Humboldt-Universität zu Berlin (Germany). Email: andreas.opitz@hu-berlin.de.
b. Helmholtz-Zentrum Berlin für Materialien und Energie (Germany).
c. Institut für Chemie and IRIS Adlershof, Humboldt-Universität zu Berlin (Germany).
d. Institut für Angewandte Physik, Universität Tübingen (Germany).
e. Experimentelle Physik VI, Universität Würzburg (Germany).
f. School of Chemistry and Biochemistry and Center for Organic Photonics and Electronics (COPE), Georgia Institute of Technology Atlanta (USA).
* Corresponding author

Abstract

The electrical and optoelectronic properties of organic semiconductor thin films can be tailored by mixing two molecular materials, e.g., by co-deposition. Possible resulting morphologies include phase separation or mixed crystals, which can form either solid solutions or ordered complexes, but it is difficult to predict *a priori* the morphology that will result for a given material combination. Here, we study electron transfer between planar electron donor molecules and a non-planar electron acceptor in co-deposited films by analyzing morphological, vibrational and optical properties. For the donor under study here that do not undergo ground-state electron transfer to the acceptor we find phase separation in mixed film. If ground-state electron transfer is present, the balance between crystal binding energy of the single component materials and the Coulomb attraction between ions formed in the co-deposited film drives the co-deposited films either into phase separation or mixed crystal formation. To rationalize the resulting morphology of these co-deposited films within the laws of thermodynamics, it is necessary to consider structural incompatibility of the molecules as well as the Coulomb attraction between molecular ions, when formed via ground-state electron transfer.

Introduction

Co-deposition of molecular materials is a widespread approach to tune electrical and optoelectronic properties of functional thin films in multilayer devices. For instance, molecules with efficient

† Present address: Energy Materials Laboratory, Centre for Nano and Soft Matter Sciences, Jalahalli, Bengaluru (India)
‡ Present address: Environmental Science and New Energy Technology Center (Center 1), Shenzhen Geim Graphene Center (SGC), Tsinghua-Berkeley Shenzhen Institute (TBSI), Tsinghua University, (China)
§ Present address: Fachbereich Physik, Freie Universität Berlin (Germany)
** Present address: DWI-Leibniz Institute for Interactive Materials, Aachen (Germany) and Institute of Technical and Macromolecular Chemistry, RWTH Aachen University (Germany)
†† Present address: Nanostructured Materials Department, Material Science Institute of Barcelona (ICMAB-CSIC, Spain)

phosphorescence or thermally-activated delayed fluorescence are uniformly distributed into amorphous films of the molecular charge-transport material in organic light emitting diodes (OLEDs). [1–3] Charge-transport layers in OLEDs or organic photovoltaic cells (OPVCs) often contain dopant molecules, ideally uniformly distributed, to increase the charge-carrier density and therefore electrical conductivity. [4] Films comprising phase-separated moieties of electron-donor and -acceptor molecules are preferred in the active layer of OPVCs for efficient charge separation and collection subsequent to optical excitation. [5,6]

The different morphologies of thin films formed by co-deposition *via* vacuum sublimation of molecular materials can partly be rationalized by thermodynamic considerations following Flory and Huggins, at least in the limit of low growth rates, i.e. near equilibrium. [7,8] Taking materials A and B, the change of free energy upon mixing, resulting from the balance of entropy increase and internal energy decrease, is given by [9,10]

$$\Delta F_{\mathrm{mix}} = k_{\mathrm{B}}T \cdot (x_{\mathrm{A}} \cdot \ln x_{\mathrm{A}} + x_{\mathrm{B}} \cdot \ln x_{\mathrm{B}} + \chi \cdot x_{\mathrm{A}}x_{\mathrm{B}}), \quad (1)$$

where k_{B} is the Boltzmann constant, T is the temperature, and x_{A}, x_{B} are the relative concentrations. The dimensionless interaction parameter χ is defined *via* the energies of interaction between molecules of the same type (W_{AA}, W_{BB}) and between different molecules (W_{AB}) as [9]

$$\chi = {}^{Z}/_{k_{\mathrm{B}}T}\,(W_{\mathrm{AA}} + W_{\mathrm{BB}} - 2W_{\mathrm{AB}}), \quad (2)$$

with Z as coordination number. Depending on the interaction parameter χ, the morphologies of co-deposited films can be distinguished in the simplest approach following the categorization by Kitaigorodsky [9] as

- mixed crystals as ordered complexes ($\chi < 0$),
- mixed crystals as solid solutions ($\chi \approx 0$), and
- phase separation ($\chi > 2$).

Kitaigorodsky summarized in 1984, that isoelectronicity and isostructurality is important to form mixed crystals. [9] This means that molecules should have similar chemical and crystal structures, especially similarly sized π-systems, which increases the energy of interaction W_{AB} due to strong π-orbital overlap. [11–13] Additionally, equations 1 & 2 need to be extended for crystalline materials composed of anisotropic molecules, and direction-dependent terms have to be included. [13] Further complexity is added if limited surface diffusion and fast nucleation are induced by the growth conditions, which may result in a non-equilibrium film structure, even for a single-component material. [14,15] The growth kinetics are thus even more complex for co-deposited films, especially if structural incompatibility and steric hindrance of the molecules are present.

It thus appears that one way to realize mixed crystals as ordered complexes is to combine suitably chosen electron-donor and -acceptor molecules. [16,17] This has been reported for prototypical planar donor molecules, including pentacene, diindenoperylene, oligothiophene, benzothieno-benzothiophene, and dibenzotetrathiafulvalene, with planar acceptor molecules of the tetracyano-quinodimethane and tetracyanonaphthoquinodimethane family, as well as for pentacene with perfluoropentacene. [18–22] Solid solutions have been reported for co-deposited films of sexithiophene

(6T) with dihexyl-6T or its perfluorinated versions, silylethynylated acenes and N-heteroacenes, as well as for phthalocyanines and their perfluorinated versions. [23–27] Co-deposition of planar molecules, such as 3,4,9,10-perylenetetracarboxylic-bis-benzimidazole, hexabenzocoronenes, phthalocyanine, oligo-thiophene, pentacene and diindenoperylene, with non-planar fullerenes [6,28–33] resulted in phase separation due to structural dissimilarity, however, with kinetic limitations.[33] Phase separation due to structural incompatibility was reported for co-deposited films of planar molecules with different sizes of the π-conjugated systems such as sexi- and quarterthiophene, and pentacene and dihexyl-sexithiophene or 3,4,9,10-perylenetetracarboxylic-bis-benzimidazole. [12,34]

Within this study, we focus on molecule pairs that potentially undergo ground-state electron transfer, which is highly relevant for doping of organic semiconductors. Diindenoperylene (DIP), pentacene (Pen), and dibenzotetrathiafulvalene (DBTTF) are used as planar donor molecules and molybdenum tris[1,2-bis(trifluoromethyl)ethane-1,2-dithiolene] [$Mo(tfd)_3$] as a strong, non-planar acceptor with a pinwheel-like structure. The chemical structures are given in Figure 1a. Structural dissimilarity, meaning differences in size, shape, and planarity, [9,35] is thus apparent for our planar donor molecules in conjunction with the non-planar acceptor molecule $Mo(tfd)_3$. We characterize structural, vibrational and optical properties of co-deposited films and relate those to the relative energy levels. Experimental details are given in the Supporting Information (SI).

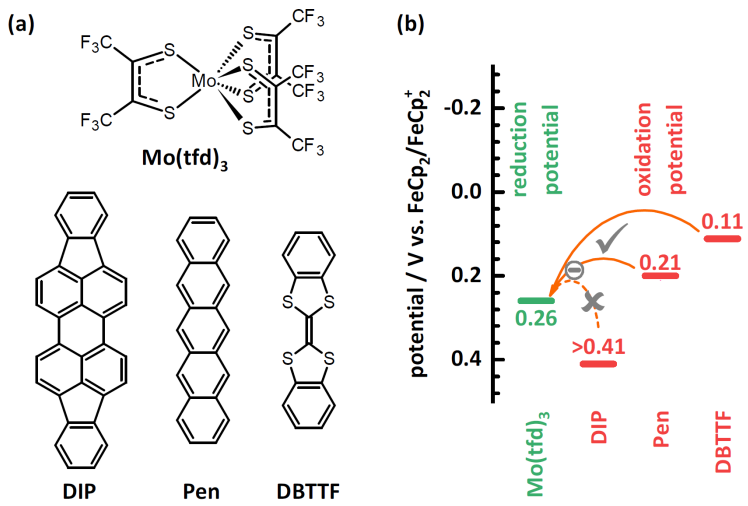

Figure 1: (a) Chemical structures of molybdenum tris[1,2-bis(trifluoromethyl)ethane-1,2-dithiolene] [$Mo(tfd)_3$], diindenoperylene (DIP), pentacene (Pen), and dibenzotetrathiafulvalene (DBTTF). (b) Redox potentials determined by cyclic voltammetry in solution referenced to the ferrocene/ferrocenium ($FeCp_2/FeCp_2^+$) redox couple. Voltammograms for DIP, Pen, and DBTTF are given in the SI. The data for $Mo(tfd)_3$ are taken from literature. [36] The arrows show energetically favorable electron transfer from DBTTF and Pen to $Mo(tfd)_3$ molecules. The electron transfer from DIP to $Mo(tfd)_3$ is forbidden.

Results

Figure 1b shows the oxidation potentials of the donor materials determined here, all referenced to the ferrocene/ferrocenium redox couple. The reduction potential of $Mo(tfd)_3$ is taken from literature [36], as well as the oxidation potential of DBTTF. [21] $Mo(tfd)_3$ shows reversible reduction and DBTTF reversible

oxidation processes. Extended effort was necessary to determine the oxidation potentials of DIP and Pen due to low solubility and their proneness to form dimers after charging. [37] The given value for DIP should be regarded as a lower boundary determined from the measured potential, as the standard potential can be up to 350 mV higher following the Nernst equation due to a possible subsequent dimerization of DIP radical cations. [37] The cyclic voltammograms for DBTTF and DIP, their differential pulse voltammograms, and other details of their oxidation processes are given in the SI. In our case, the reduction potential E_{red} of the acceptor is higher than the oxidation potential E_{ox} of DIP, and lower than E_{ox} of Pen and DBTTF, yielding the sequence $E_{ox,DIP} > E_{red,Mo(tfd)3} > E_{ox,PEN} > E_{ox,DBTTF}$. An energetically favorable electron transfer to the acceptor $Mo(tfd)_3$ seems possible for DBTTF and Pen as E_{ox} for these molecules is clearly more negative than E_{red} of the acceptor. Ionization energy and electron affinity measured by direct and inverse photoelectron spectroscopy on thin films were reported earlier and are summarized in the SI (see Figure S15). [36,38–40] One has to keep in mind that ionization energy and electron affinity (IE and EA) are different from the gas-phase or solution-based measurements due to environment-dependent polarization. Furthermore, the values for ionization energy and electron affinity depend notably on the molecular orientation with respect to the surface in crystalline films. [41–45] Wegner et al. showed, that data from cyclic voltammetry can, at least in some cases, be more reliable than solid-state IE/EA data for prediction of electron transfer in mixed films. [46] Therefore, we use the CV data set of energy levels in the following considerations.

For the chemical equilibrium between neutral and ionized donor (D) and acceptor (A) molecules, according to

$$\mathrm{D} + \mathrm{A} \rightleftharpoons \mathrm{D}^{+} + \mathrm{A}^{-}, \tag{3}$$

the redox potential difference $\Delta E_{\mathrm{redox}} = E_{\mathrm{red}} - E_{\mathrm{ox}}$ has to be considered as the exergonicity of the electron transfer reaction. The concentrations of neutral molecules $c^2_{\mathrm{neutral}} = c_{\mathrm{D}} \cdot c_{\mathrm{A}}$ and of charged molecules $c^2_{\mathrm{charged}} = c_{\mathrm{D}^+} \cdot c_{\mathrm{A}^-}$ for equimolar stoichiometry can be related by the equilibrium constant K to $\Delta E_{\mathrm{redox}}$ as [46]

$$\Delta E_{\mathrm{redox}} {}^{F}\!/_{RT} = \ln K = \ln {}^{c_{\mathrm{D}^+} \cdot c_{\mathrm{A}^-}}\!/_{c_{\mathrm{D}} \cdot c_{\mathrm{A}}} = 2 \cdot \ln {}^{c_{\mathrm{charged}}}\!/_{c_{\mathrm{neutral}}}. \tag{4}$$

Here F is the Faraday constant, R the universal gas constant, and T the temperature.

The large negative redox offset for $Mo(tfd)_3$ and DIP ($\Delta E_{redox} \geq -0.15$ V) prohibits substantial electron transfer from DIP to $Mo(tfd)_3$ $\left({}^{c_{\mathrm{charged}}}\!/_{c_{\mathrm{neutral}}} \leq 5 \cdot 10^{-2}\right)$ at room temperature (290 K). Electron transfer from Pen to $Mo(tfd)_3$ and ion pair formation should be possible with $\Delta E_{redox} = +0.05$ V $\left({}^{c_{\mathrm{charged}}}\!/_{c_{\mathrm{neutral}}} \approx 3\right)$. $Mo(tfd)_3$ and DBTTF yield an even more positive redox potential difference ($\Delta E_{redox} = +0.15$ V), giving a strong driving force for electron transfer $\left({}^{c_{\mathrm{charged}}}\!/_{c_{\mathrm{neutral}}} \approx 20\right)$.

The concentration ratios given above are estimates for the interaction taking place between individual donor and acceptor molecules. The values may well differ in the presence of another solvent or in thin films. However, this estimate provides a reference point for the observations discussed further below.

The morphology of single-component and co-deposited films was characterized by scanning force microscopy. The corresponding images are shown in Figure 2. The single-component films of the

donors and the acceptor are polycrystalline in nature and show typical crystallite sizes and shapes as reported in literature. [47–49] The surfaces of co-deposited films of DIP:$Mo(tfd)_3$ and Pen:$Mo(tfd)_3$, both with equimolar ratio, exhibit a similar appearance but with plate-like and elongated structures present within the film and at the surface. Except for these, the surface morphology resembles that of the single-component donor films, which is why we attribute the additional, elongated plate-like structures present in both co-deposited films to $Mo(tfd)_3$. X-ray reflectivity data for single-component DIP and co-deposited DIP:$Mo(tfd)_3$ films are given in the SI (see Figure S16), showing the presence of DIP crystallites in the co-deposited film with the same lattice spacing in both films. [50] This assignment from morphology and the results from X-ray reflectivity indicate phase separation in co-deposited films of DIP:$Mo(tfd)_3$ and Pen:$Mo(tfd)_3$. The single-component DBTTF film and the co-deposited film containing DBTTF and $Mo(tfd)_3$ in a 10:1 molar ratio exhibits highly similar morphology, featuring large area and flat crystallites. If phase separation persisted also for this material pair, the $Mo(tfd)_3$ molecules might be accumulated at the edges of the observed crystallites, which we do not clearly observe here. Incorporation of $Mo(tfd)_3$ molecules into the DBTTF layer is also a possibility due to a non-vanishing solubility. In contrast, the morphology of the equimolar co-deposited DBTTF:$Mo(tfd)_3$ film is defined by apparently rather large crystallites and bare substrate regions in between. The individual molecular compounds DBTTF and $Mo(tfd)_3$ cannot, therefore, be distinguished in co-deposited films in either molar ratio.

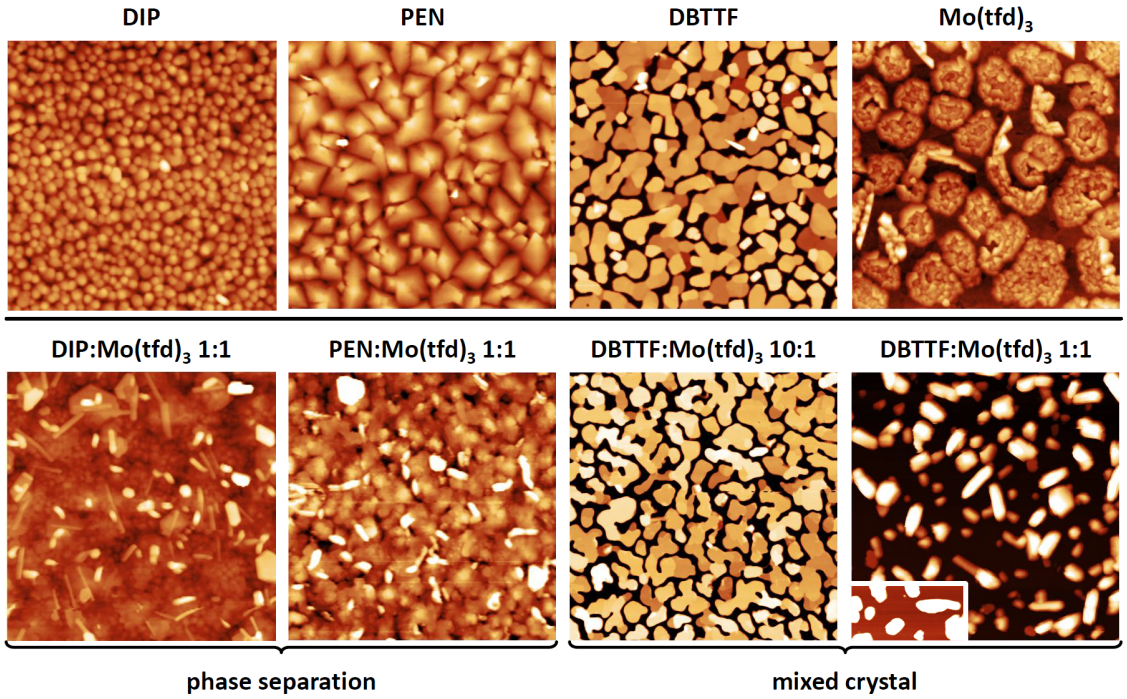

Figure 2: Scanning force micrographs for single-component and equimolar co-deposited films of DIP, Pen, DBTTF, and $Mo(tfd)_3$. Additionally, the co-deposited film of DBTTF:$Mo(tfd)_3$ with a molar ratio of 10:1 is shown. The color scale was modified in the lower left corner of the micrograph to visualize the bare substrate between the crystallites of the equimolar co-deposited DBTTF:$Mo(tfd)_3$ film. The size for all images is 4×4 µm². Different height scales are applied.

While we conclude that there is phase separation for co-deposited DIP:$Mo(tfd)_3$ and Pen:$Mo(tfd)_3$, the formation of a mixed crystal for DBTTF:$Mo(tfd)_3$ may be assumed, even if structural dissimilarity between the involved molecules is evident. Two distinct morphologies are observed for the low and high $Mo(tfd)_3$ content. The coexistence of both morphologies is found in the same sample for an intermediate molar ratio of 4:1, as shown in the SI (see Figure S17). Accordingly, and in conjunction with further considerations discussed further below, we relate the morphology of the equimolar co-deposited film to an ordered donor-acceptor complex.

Raman spectra of single-component and co-deposited films are depicted in Figure 3. The four main vibrational features of DIP and Pen observed in single-component films can be assigned to in-plane vibrations as combination of C–C stretching motion with C–H bending. [51,52] DBTTF exhibits a totally symmetric stretching vibrational mode of the central C=C bond at about 1542 cm^{-1}. [53,54] The stretching mode of perturbed C=C bonds of the dithiolene ligands of $Mo(tfd)_3$ is reported to appear around 1461 cm^{-1}. [55,56] The three additionally marked features for DBTTF and the lower wavenumber features for $Mo(tfd)_3$ are reported in literature, [53–56] although without assignment. The spectra for co-deposited films of $Mo(tfd)_3$ with DIP and Pen are a linear combination of the features of the single-component films, with slight broadening and negligible peak shifts. For DIP:$Mo(tfd)_3$ both molecular species contribute with similar intensity to the Raman spectrum. In contrast, the Raman cross-section of Pen seems to be much lower than that of $Mo(tfd)_3$ or DIP, as mainly $Mo(tfd)_3$ signatures are detected in the equimolar co-deposited film and the strongest Pen signature at 1376 cm^{-1} appears with low intensity only.

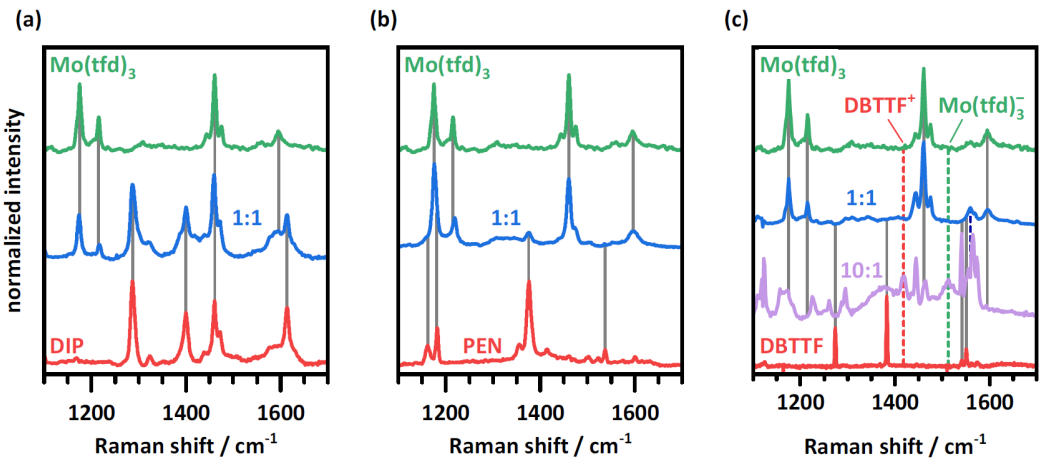

Figure 3: Raman spectra of single-component (a) DIP, (b) Pen, and (c) DBTTF and a single-component $Mo(tfd)_3$ films, as well as co-deposited D:A films. The spectra are shifted vertically for clarity. The spectra were recorded for equimolar DIP:$Mo(tfd)_3$ and PEN:$Mo(tfd)_3$, and molar ratios of 1:1 and 10:1 for DBTTF:$Mo(tfd)_3$. The grey lines indicate the peak position for single-component samples. The assignment of vibrational features related to the $Mo(tfd)_3$ anion (green dashed line) and the DBTTF cation (red dashed line), as well as the feature at around 1560 cm^{-1} (dark blue dashed line) is taken from literature. [53–56]

The spectrum of the equimolar DBTTF:$Mo(tfd)_3$ film is dominated by the $Mo(tfd)_3$ signatures with DBTTF features that are barely noticeable. However, around 1560 cm^{-1} additional peaks appear, which

are absent in the single-component films. The DBTTF:$Mo(tfd)_3$ film with a molar ratio of 10:1 shows significant differences in the Raman spectrum in comparison to the spectra of single-component DBTTF and $Mo(tfd)_3$ films, and also to the spectrum of the equimolar mixed film. Again, features around 1560 cm^{-1} are present. The wavenumber of the totally symmetric stretching vibrational mode of the central C=C bond in the DBTTF cation is at 1419 cm^{-1}, [53,54] and the stretching mode of perturbed C=C bonds of dithiolene ligands for $Mo(tfd)_3$ anions is at 1513 cm^{-1}. [55,56] Raman peaks are present at these two wavenumbers in the co-deposited DBTTF:$Mo(tfd)_3$ film (as marked in Figure 3c), and they are absent in the single-component films of DBTTF and $Mo(tfd)_3$.

The fact that Raman spectra of the co-deposited films of DIP and PEN with $Mo(tfd)_3$ are a superposition of the single-component DIP, Pen and $Mo(tfd)_3$ films is in line with phase separation, as already deduced from the morphology. Evidence for electronic interaction, e.g., charge transfer, is not found. In contrast, new features appear for co-deposited films of DBTTF and $Mo(tfd)_3$ that can be assigned to DBTTF cations and $Mo(tfd)_3$ anions. This is consistent with the ground-state electron transfer from DBTTF to $Mo(tfd)_3$ anticipated from the redox potentials (*vide supra*). The clear presence of vibrational peaks related to the ionic species is given only for the molar ratio of 10:1, whereas the equimolar co-deposited film is dominated by the vibrational features of the neutral $Mo(tfd)_3$. The portion of charged $Mo(tfd)_3$ molecules in relation to all $Mo(tfd)_3$ molecules is higher for the lower amount of acceptor molecules present in the film. This is most likely due to the different morphologies observed by scanning force microscopy for the co-deposited films with molar ratios of 10:1 and 1:1, as shown above. Although, from an energetic point of view, electron transfer also appears feasible for Pen:$Mo(tfd)_3$, clear features of Pen cations and $Mo(tfd)_3$ anions were not seen in Raman spectra. Taking into account that phase separation prevails for Pen:$Mo(tfd)_3$, the relevant volume in which electron transfer may happen is limited to grain boundaries, and thus the pertinent signal may be too low to be observed by Raman spectroscopy.

Further support for the assignments made in preceding paragraphs come from UV-vis-NIR absorption spectroscopy. Spectra of single-component DIP, Pen, DBTTF and $Mo(tfd)_3$ films (see Figure 4) reveal the lowest absorption energy for DIP at ca. 2.2 eV, for PEN at ca. 1.8 eV, and for DBTTF at ca. 3.0 eV, which is - together with the overall spectral shape - in agreement with literature. [21,57,58] Absorption spectra for $Mo(tfd)_3$ films have not yet been reported. The lowest transition energy is at ca. 2.1 eV in films, as well as in chloroform solution (see SI, Figure S2). This energy is comparable to the value given for other solvents. [36,59] To check for the occurrence of radical cations and anions, the absorption signatures of ionic molecules were measured in solution upon doping with different inorganic salts. [36,46,60–63] Details on the data obtained by spectroelectrochemistry are given in the SI (see Figure S3-S12).

The absorption spectrum for the equimolar DIP:$Mo(tfd)_3$ is displayed in Figure 4a. The main absorption features of the co-deposited film can be readily described by absorption of single-component DIP and $Mo(tfd)_3$ films. Small solvatochromic shifts occur due to the change of the dielectric environment in co-deposited films. No sub-gap absorption for DIP:$Mo(tfd)_3$ is observed, as seen from the magnified inset. The feature between 1.40 and 1.50 eV is an artifact from the measurement setup due to detector and grating change. The absorption spectrum of Pen:$Mo(tfd)_3$ (see Figure 4b) also shows the absorption features of the respective single-component films, slightly shifted due to the different dielectric environment. Additionally, two small peaks were detected for the co-deposited film, one at

1.26 eV and, in comparison, a broader one around 1.35 eV. These stem from absorption of Pen cations and $Mo(tfd)_3$ anions (for comparison see SI Figure S2). [36,46,64] The strongest absorption feature of the $Mo(tfd)_3$ anions at about 1.8 eV coincides with the first absorption peak of neutral Pen in thin films. The presence of absorption related to Pen cations and $Mo(tfd)_3$ anions evidences electron transfer between the molecules, in line with the considerations deduced from the redox potentials above. The fraction of ions is, however, rather small. Considering the phase separation in Pen:$Mo(tfd)_3$, the electron transfer is likely limited to the grain boundaries between Pen and $Mo(tfd)_3$ crystallites. This small interaction volume results in the low intensity features of ionic Pen and $Mo(tfd)_3$ molecules.

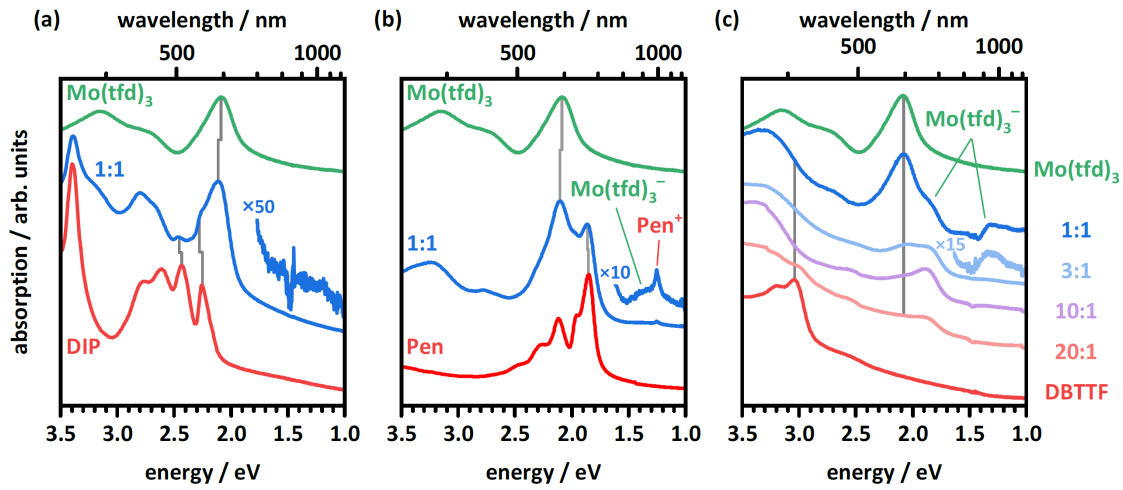

Figure 4: UV-vis-NIR absorption spectra of single-component films of (a) DIP and (b) Pen together with the spectra of a single-component $Mo(tfd)_3$ film and equimolar co-deposited D:A films. (c) shows the spectra for single-component and a series and co-deposited films containing DBTTF and $Mo(tfd)_3$ with different molar ratios. The spectra are shifted vertically for clarity. The grey lines show the position of the strongest absorption peaks related to the individual materials in the singly- and co-deposited films. The features exclusively related to absorption of $Mo(tfd)_3$ radical anions and Pen radical cations are marked. The magnified spectra are shown after background subtraction.

UV-vis-NIR absorptions spectra for DBTTF:$Mo(tfd)_3$ co-deposited films with different molar ratios are shown in Figure 4c. Absorption spectra for DBTTF and $Mo(tfd)_3$ in solution are given in the SI for comparison (see Figure S18). Absorption at 1.83 eV and at ca. 1.35 eV are due to the presence of $Mo(tfd)_3$ anions. The absorption of the DBTTF cation is in the same energy range as the strong absorption of the $Mo(tfd)_3$ anion, but much lower in intensity. This is inferred from comparison with the absorption of DBTTF cations in solution (see SI Figure S2 and S4). Notably, the strong absorption feature of DBTTF cations in the range between 2.5 eV and 3.0 eV measured in solution is absent in thin films. This might be due to molecular ordering leading to a preferred orientation of transition dipole moments within the films, in contrast to their randomized orientations in solution. Nearly complete ionization of the added $Mo(tfd)_3$ seems to be present for molar ratios of 20:1 and 10:1, as only the absorption feature of $Mo(tfd)_3$ anions is detected. For higher acceptor contents the absorption features of neutral $Mo(tfd)_3$ become visible as well. This is agreement with the results obtained by Raman spectroscopy and might be related to the before mentioned differences in film morphology.

The detected amount of charged molecules for co-deposited films of DBTTF and $Mo(tfd)_3$ is larger than for co-deposited films of Pen and $Mo(tfd)_3$, as predicted from the redox potential differences.

To examine the effect of ground-state electron transfer between DBTTF and $Mo(tfd)_3$, i.e., doping, on charge transport, the conductivity of co-deposited films was measured with two-terminal in-plane device geometry (Figure 5). An increase in conductivity of up to five orders of magnitude for a molar ratio of 10:1 is found. At this ratio, the morphology of the co-deposited film is comparable to that of the single-component DBTTF film. However, due to the applied numbers of molar ratios, the conductivity might be higher at other ratios in this range. The morphology for larger $Mo(tfd)_3$ content, which consists of large individual crystallites (see Fig. 2) reduces the number of conducting pathways. This counteracts the increased charge carrier density and reduces the overall conductivity.

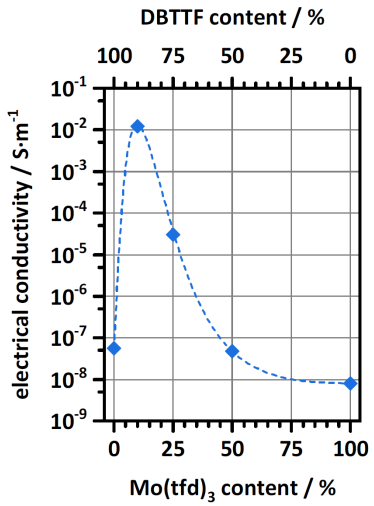

Figure 5: Dependence of the conductivity on the molar ratio for co-deposited films of DBTTF and $Mo(tfd)_3$. The dashed line is a guide to the eye.

Discussion and conclusion

Phase separation is observed here for co-deposited films of planar DIP and non-planar $Mo(tfd)_3$ molecules. Phase separation was reported for co-deposited films of DIP with the weaker and spherical acceptor C_{60}. [30,33] Spectral signatures of ions are absent in vibrational and absorption spectroscopy. Phase separation is also concluded to occur for co-deposited films of Pen and $Mo(tfd)_3$. Here, a small amount of ion pairs is present as detected by absorption spectroscopy. Most probably the electron transfer takes place at the grain boundaries in the phase-separated film. The appearance of phase separation and the presence of very weak ionic absorption features was also reported for co-deposited films of 6T:$Mo(tfd)_3$, with a redox potential difference of +0.18 V. [46] This redox potential difference is located between the values for DIP:$Mo(tfd)_3$ and Pen:$Mo(tfd)_3$ combinations. In contrast to ion pair formation, a theoretically predicted charge-transfer complex between Pen and $Mo(tfd)_3$ was reported in literature (see supporting information in [65]). We do not observe any support of this prediction in our experiment.

By contrast, no indications for phase separation are found for co-deposited films of DBTTF and $Mo(tfd)_3$. The binary film morphology found for different molar ratios indicate the formation of mixed DBTTF:$Mo(tfd)_3$ crystals, most probably stoichiometric, despite the structural dissimilarity of the two molecules. As ions must be present in the mixed-crystal structure, the co-deposited film has to be considered as an ordered donor-acceptor complex with (statistically distributed) ions or ion pairs. The interactions between the dissimilar molecules – including the Coulomb attraction between the ions present – are evidently sufficient to stabilize the mixed crystal appearing as an ordered complex without ionization of all molecules. The intermolecular integer electron transfer and the concomitant Coulomb interaction enter as additional factor to the energy W_{AB} between materials in co-deposited films, in addition to isostructurality, [9] similarities of molecular dimensions, [12,35] multipole interaction, [13] and complex formation of planar molecules with partial charge transfer [18,20]. An increase of W_{AB} leads to a reduced or possibly negative interaction parameter χ and thus allows for formation of mixed crystals as ordered complexes. The balance of W_{AA}, W_{BB}, and W_{AB} is important for the trade-off between phase separation and ordered complex formation. The interaction energies W_{AA} between the donor molecules are unknown and therefore the mentioned balance cannot be quantified here. The crystal binding energy in terms of W_{AA} of pentacene seems to be large enough to forces phase separation in co-deposited Pen:$Mo(tfd)_3$ films in the presence of integer charge transfer at grain boundaries. By the mentioned approach following Kitaigorodsky, we consider the neutral and charged species as identical compounds, differences are considered in changes of the energy of interaction between the materials. An extended model should reflect neutral and charged species of donor and acceptor as separate species and accordingly include all pairwise interaction energies. Ordered complex formation was reported for fullerenes and tetrachalcogenafulvalene molecules, partly with solvent molecules incorporated into the mixed crystal structure. [66–68] They are all described as ordered complexes with negligible or partial charge transfer.[68] The tetrachalcogenafulvalene molecules in these complexes appear in the boat confirmation. These fulvalene derivatives are non-rigid molecules and a related non-planar confirmation might also be present in the ordered complexes of DBTTF:$Mo(tfd)_3$ in our study. Complex formation between fullerene and other non-planar molecules are reported. [68] In all cases of ordered complexes containing fullerenes the non-rigid and non-planar donor molecule adapts the spherical shape of the fullerene.

In summary, electron transfer between co-deposited molecules may help drive the formation of a mixed crystal as ordered complex between planar and non-planar molecules where π-stacking is sterically hindered. This was shown here for co-deposited films of DBTTF and $Mo(tfd)_3$. The increase of interaction energy W_{AB} due to electron transfer and the resulting Coulomb energy has to be considered within the thermodynamic description. In contrast, phase separation takes place for co-deposited films of DIP and Pen with $Mo(tfd)_3$ and significant electron transfer is absent. Similar effects should thus be taken into account for co-deposited films of planar molecules, where integer charge transfer was report like in the case of zinc phthalocyanine (ZnPc) and 1,3,4,5,7,8-hexafluorotetracyano-naphtho-quinodimethane (F_6TCNNQ). [69] The current findings will help to understand the interaction behavior between differently molecular-shaped molecules and the resulting mechanism of film formation. Furthermore, the use of more complicated, e.g. ternary blends offers additional degrees of freedom such as the mixing of binary donor-acceptor films being of interests for photodetection in the infrared, not easy to implement by just one single molecular compound. [70]

Conflicts of interest

There are no conflicts to declare.

Author contributions

AO and NK initiated the study and supervised the work. CP, PB, HSSRM & BW prepared films by vacuum deposition and performed the analysis by absorption and morphology measurements. AR prepared films by sequential deposition and analyzed these. XX, VB, CK, JP performed Raman measurements. JP collected X-ray reflectivity data. TF & AO conducted solution-based absorption measurements. LG was responsible for cyclic voltammetry measurements and YZ synthesized the acceptor molecule. AH, FS, SH, SB & SRM supported the work at different stages. AO prepared the manuscript draft and all authors contributed to finalize the manuscript.

Supporting Information

The Supporting Information is available free of charge.

Experimental details, Supporting discussions and figure on absorption spectra of neutral donor molecules in solution, absorption spectra of charged molecules using inorganic dopants in solution, cyclic voltammetry and spectroelectrochemistry of donor molecules in solution, discussion on the oxidation of perylene and DIP, absorption spectra of DIP films with inorganic salts, energy levels determined by direct and inverse photoelectron spectroscopy, absorption of DBTTF and $Mo(tfd)_3$ in solution

Acknowledgements

The work was supported financially by Deutsche Forschungsgemeinschaft (OP159/2, SCHR700/20, project numbers 239543752, and GRK 2112). XX and SRM acknowledge Alexander-von-Humboldt Foundation for support. YZ, SB and SRM thank the U.S. National Science foundation for support of this work, under award No. DMR-1729737. The authors thank Stephan Lüdtke for experimental support.

References

(1) Volz, D. Review of Organic Light-Emitting Diodes with Thermally Activated Delayed Fluorescence Emitters for Energy-Efficient Sustainable Light Sources and Displays. *J. Photonics Energy* **2016**, *6* (2), 020901. https://doi.org/10.1117/1.JPE.6.020901.

(2) Minaev, B.; Baryshnikov, G.; Agren, H. Principles of Phosphorescent Organic Light Emitting Devices. *Phys. Chem. Chem. Phys.* **2014**, *16* (5), 1719–1758. https://doi.org/10.1039/C3CP53806K.

(3) Shirota, Y.; Kageyama, H. Organic Materials for Optoelectronic Applications: Overview. *Handb. Org. Mater. Electron. Photonic Devices* **2019**, 3–42. https://doi.org/10.1016/B978-0-08-102284-9.00001-2.

(4) Walzer, K.; Maennig, B.; Pfeiffer, M.; Leo, K. Highly Efficient Organic Devices Based on Electrically Doped Transport Layers. *Chem. Rev.* **2007**, *107* (4), 1233–1271. https://doi.org/10.1021/cr050156n.

(5) Forrest, S. R. The Limits to Organic Photovoltaic Cell Efficiency. *MRS Bull.* **2005**, *30* (1), 28–32. https://doi.org/10.1557/mrs2005.5.

(6) Rand, B. P.; Genoe, J.; Heremans, P.; Poortmans, J. Solar Cells Utilizing Small Molecular Weight

Organic Semiconductors. *Prog. Photovoltaics Res. Appl.* **2007**, *15* (8), 659–676. https://doi.org/10.1002/pip.788.
(7) Flory, P. J. Thermodynamics of High Polymer Solutions. *J. Chem. Phys.* **1941**, *9* (8), 660–661. https://doi.org/10.1063/1.1750971.
(8) Huggins, M. L. Solutions of Long Chain Compounds. *J. Chem. Phys.* **1941**, *9* (5), 440. https://doi.org/10.1063/1.1750930.
(9) Kitaigorodsky, A. I. *Mixed Crystals*; Springer Series in Solid-State Sciences; Springer Berlin Heidelberg: Berlin, Heidelberg, 1984; Vol. 33. https://doi.org/10.1007/978-3-642-81672-7.
(10) Strobl, G. Polymer Blends and Block Copolymers. In *The Physics of Polymers*; Springer: Berlin Heidelberg New York, 2007; pp 105–164. https://doi.org/10.1007/978-3-540-68411-4_4.
(11) Hinderhofer, A.; Schreiber, F. Organic-Organic Heterostructures: Concepts and Applications. *ChemPhysChem* **2012**, *13* (3), 628–643. https://doi.org/10.1002/cphc.201100737.
(12) Vogel, J.-O.; Salzmann, I.; Duhm, S.; Oehzelt, M.; Rabe, J. P.; Koch, N. Phase-Separation and Mixing in Thin Films of Co-Deposited Rod-like Conjugated Molecules. *J. Mater. Chem.* **2010**, *20* (20), 4055–4066. https://doi.org/10.1039/b927594k.
(13) Aufderheide, A.; Broch, K.; Novák, J.; Hinderhofer, A.; Nervo, R.; Gerlach, A.; Banerjee, R.; Schreiber, F. Mixing-Induced Anisotropic Correlations in Molecular Crystalline Systems. *Phys. Rev. Lett.* **2012**, *109* (15), 156102. https://doi.org/10.1103/PhysRevLett.109.156102.
(14) Cao, Z. *Thin Film Growth: Physics, Materials Science and Applications*; Woodhead Pub Ltd, 2011.
(15) Forrest, S. R. Ultrathin Organic Films Grown by Organic Molecular Beam Deposition and Related Techniques. *Chem. Rev.* **1997**, *97* (6), 1793–1896. https://doi.org/10.1021/cr941014o.
(16) Mulliken, R. S.; Person, W. B. Donor-Acceptor Complexes. *Annu. Rev. Phys. Chem.* **1962**, *13* (1), 107–126. https://doi.org/10.1146/annurev.pc.13.100162.000543.
(17) Briegleb, G. *Elektronen-Donator-Acceptor-Komplexe*; Springer Berlin Heidelberg: Berlin, Heidelberg, 1961. https://doi.org/10.1007/978-3-642-86555-8.
(18) Duva, G.; Pithan, L.; Zeiser, C.; Reisz, B.; Dieterle, J.; Hofferberth, B.; Beyer, P.; Bogula, L.; Opitz, A.; Kowarik, S.; Hinderhofer, A.; Gerlach, A.; Schreiber, F. Thin-Film Texture and Optical Properties of Donor/Acceptor Complexes. Diindenoperylene/F6TCNNQ vs Alpha-Sexithiophene/F6TCNNQ. *J. Phys. Chem. C* **2018**, *122* (32), 18705–18714. https://doi.org/10.1021/acs.jpcc.8b03744.
(19) Méndez, H.; Heimel, G.; Winkler, S.; Frisch, J.; Opitz, A.; Sauer, K.; Wegner, B.; Oehzelt, M.; Röthel, C.; Duhm, S.; Többens, D.; Koch, N.; Salzmann, I. Charge-Transfer Crystallites as Molecular Electrical Dopants. *Nat. Commun.* **2015**, *6* (1), 8560. https://doi.org/10.1038/ncomms9560.
(20) Méndez, H.; Heimel, G.; Opitz, A.; Sauer, K.; Barkowski, P.; Oehzelt, M.; Soeda, J.; Okamoto, T.; Takeya, J.; Arlin, J. B.; Balandier, J. Y.; Geerts, Y.; Koch, N.; Salzmann, I. Doping of Organic Semiconductors: Impact of Dopant Strength and Electronic Coupling. *Angew. Chemie - Int. Ed.* **2013**, *52* (30), 7751–7755. https://doi.org/10.1002/anie.201302396.
(21) Beyer, P.; Pham, D.; Peter, C.; Koch, N.; Meister, E.; Brütting, W.; Grubert, L.; Hecht, S.; Nabok, D.; Cocchi, C.; Draxl, C.; Opitz, A. State-of-Matter-Dependent Charge-Transfer Interactions between Planar Molecules for Doping Applications. *Chem. Mater.* **2019**, *31* (4), 1237–1249. https://doi.org/10.1021/acs.chemmater.8b01447.
(22) Salzmann, I.; Duhm, S.; Heimel, G.; Rabe, J. P.; Koch, N.; Oehzelt, M.; Sakamoto, Y.; Suzuki, T. Structural Order in Perfluoropentacene Thin Films and Heterostructures with Pentacene. *Langmuir* **2008**, *24* (14), 7294–7298. https://doi.org/10.1021/la800606h.
(23) Reisz, B.; Weimer, S.; Banerjee, R.; Zeiser, C.; Lorch, C.; Duva, G.; Dieterle, J.; Yonezawa, K.; Yang, J.-P. P.; Ueno, N.; Kera, S.; Hinderhofer, A.; Gerlach, A.; Schreiber, F. Structural, Optical, and Electronic Characterization of Perfluorinated Sexithiophene Films and Mixed Films with Sexithiophene. *J. Mater. Res.* **2017**, *32* (10), 1908–1920. https://doi.org/10.1557/jmr.2017.99.

(24) Vogel, J.-O.; Salzmann, I.; Opitz, R.; Duhm, S.; Nickel, B.; Rabe, J. P.; Koch, N. Sub-Nanometer Control of the Interlayer Spacing in Thin Films of Intercalated Rodlike Conjugated Molecules. *J. Phys. Chem. B* **2007**, *111* (51), 14097–14101. https://doi.org/10.1021/jp077158r.
(25) Schwarze, M.; Tress, W.; Beyer, B.; Gao, F.; Scholz, R.; Poelking, C.; Ortstein, K.; Gunther, A. A.; Kasemann, D.; Andrienko, D.; Leo, K. Band Structure Engineering in Organic Semiconductors. *Science* **2016**, *352* (6292), 1446–1449. https://doi.org/10.1126/science.aaf0590.
(26) Xu, X.; Xiao, T.; Gu, X.; Yang, X.; Kershaw, S. V.; Zhao, N.; Xu, J.; Miao, Q. Solution-Processed Ambipolar Organic Thin-Film Transistors by Blending p- and n-Type Semiconductors: Solid Solution versus Microphase Separation. *ACS Appl. Mater. Interfaces* **2015**, *7* (51), 28019–28026. https://doi.org/10.1021/acsami.5b01172.
(27) Lucia, E. A.; Verderame, F. D. Spectra of Polycrystalline Phthalocyanines in the Visible Region. *J. Chem. Phys.* **1968**, *48* (6), 2674–2681. https://doi.org/10.1063/1.1669501.
(28) Veenstra, S. C.; Malliaras, G. G.; Brouwer, H. J.; Esselink, F. J.; Krasnikov, V. V.; van Hutten, P. F.; Wildeman, J.; Jonkman, H. T.; Sawatzky, G. A.; Hadziioannou, G. Sexithiophene-C60 Blends as Model Systems for Photovoltaic Devices. *Synth. Met.* **1997**, *84* (1–3), 971–972. https://doi.org/10.1016/S0379-6779(96)04235-X.
(29) Salzmann, I.; Duhm, S.; Opitz, R.; Johnson, R. L.; Rabe, J. P.; Koch, N. Structural and Electronic Properties of Pentacene-Fullerene Heterojunctions. *J. Appl. Phys.* **2008**, *104* (11), 114518. https://doi.org/10.1063/1.3040003.
(30) Wagner, J.; Gruber, M.; Hinderhofer, A.; Wilke, A.; Bröker, B.; Frisch, J.; Amsalem, P.; Vollmer, A.; Opitz, A.; Koch, N.; Schreiber, F.; Brütting, W. High Fill Factor and Open Circuit Voltage in Organic Photovoltaic Cells with Diindenoperylene as Donor Material. *Adv. Funct. Mater.* **2010**, *20* (24), 4295–4303. https://doi.org/10.1002/adfm.201001028.
(31) Uchida, S.; Xue, J.; Rand, B. P.; Forrest, S. R. Organic Small Molecule Solar Cells with a Homogeneously Mixed Copper Phthalocyanine: C60 Active Layer. *Appl. Phys. Lett.* **2004**, *84* (21), 4218–4220. https://doi.org/10.1063/1.1755833.
(32) Wong, W. W. H.; Singh, T. B.; Vak, D.; Pisula, W.; Yan, C.; Feng, X.; Williams, E. L.; Chan, K. L.; Mao, Q.; Jones, D. J.; Ma, C.-Q.; Müllen, K.; Bäuerle, P.; Holmes, A. B. Solution Processable Fluorenyl Hexa-Peri-Hexabenzocoronenes in Organic Field-Effect Transistors and Solar Cells. *Adv. Funct. Mater.* **2010**, *20* (6), 927–938. https://doi.org/10.1002/adfm.200901827.
(33) Banerjee, R.; Novák, J.; Frank, C.; Lorch, C.; Hinderhofer, A.; Gerlach, A.; Schreiber, F. Evidence for Kinetically Limited Thickness Dependent Phase Separation in Organic Thin Film Blends. *Phys. Rev. Lett.* **2013**, *110* (18), 185506. https://doi.org/10.1103/PhysRevLett.110.185506.
(34) Peumans, P.; Uchida, S.; Forrest, S. R. Efficient Bulk Heterojunction Photovoltaic Cells Using Small-Molecular-Weight Organic Thin Films. *Nature* **2003**, *425* (6954), 158–162. https://doi.org/10.1038/nature01949.
(35) Schur, E.; Nauha, E.; Lusi, M.; Bernstein, J. Kitaigorodsky Revisited: Polymorphism and Mixed Crystals of Acridine/Phenazine. *Chem. - A Eur. J.* **2015**, *21* (4), 1735–1742. https://doi.org/10.1002/chem.201404321.
(36) Qi, Y.; Sajoto, T.; Barlow, S.; Kim, E.-G.; Brédas, J.-L.; Marder, S. R.; Kahn, A. Use of a High Electron-Affinity Molybdenum Dithiolene Complex to p-Dope Hole-Transport Layers. *J. Am. Chem. Soc.* **2009**, *131* (35), 12530–12531. https://doi.org/10.1021/ja904939g.
(37) Beitz, T.; Laudien, R.; Löhmannsröben, H.-G.; Kallies, B. Ion Mobility Spectrometric Investigation of Aromatic Cations in the Gas Phase. *J. Phys. Chem. A* **2006**, *110* (10), 3514–3520. https://doi.org/10.1021/jp055335n.
(38) Han, W. N.; Yonezawa, K.; Makino, R.; Kato, K.; Hinderhofer, A.; Murdey, R.; Shiraishi, R.; Yoshida, H.; Sato, N.; Ueno, N.; Kera, S. Quantitatively Identical Orientation-Dependent Ionization Energy and Electron Affinity of Diindenoperylene. *Appl. Phys. Lett.* **2013**, *103* (25), 253301. https://doi.org/10.1063/1.4850531.
(39) Fukagawa, H.; Yamane, H.; Kataoka, T.; Kera, S.; Nakamura, M.; Kudo, K.; Ueno, N. Origin of

the Highest Occupied Band Position in Pentacene Films from Ultraviolet Photoelectron Spectroscopy: Hole Stabilization versus Band Dispersion. *Phys. Rev. B - Condens. Matter Mater. Phys.* **2006**, *73* (24), 24–26. https://doi.org/10.1103/PhysRevB.73.245310.

(40) Sato, N.; Inokuchi, H.; Shirotani, I. Polarization Energies of Tetrathiafulvalene Derivatives. *Chem. Phys.* **1981**, *60* (3), 327–333. https://doi.org/10.1016/0301-0104(81)80168-1.

(41) Sato, N.; Inokuchi, H.; Silinsh, E. A. Reevaluation of Electronic Polarization Energies in Organic Molecular Crystals. *Chem. Phys.* **1987**, *115* (2), 269–277. https://doi.org/10.1016/0301-0104(87)80041-1.

(42) Sato, N.; Seki, K.; Inokuchi, H. Polarization Energies of Organic Solids Determined by Ultraviolet Photoelectron Spectroscopy. *J. Chem. Soc. Faraday Trans. 2 Mol. Chem. Phys.* **1981**, *77* (9), 1621–1633. https://doi.org/10.1039/F29817701621.

(43) Yoshida, H.; Yamada, K.; Tsutsumi, J.; Sato, N. Complete Description of Ionization Energy and Electron Affinity in Organic Solids: Determining Contributions from Electronic Polarization, Energy Band Dispersion, and Molecular Orientation. *Phys. Rev. B - Condens. Matter Mater. Phys.* **2015**, *92* (7), 1–13. https://doi.org/10.1103/PhysRevB.92.075145.

(44) Duhm, S.; Heimel, G.; Salzmann, I.; Glowatzki, H.; Johnson, R. L.; Vollmer, A.; Rabe, J. P.; Koch, N. Orientation-Dependent Ionization Energies and Interface Dipoles in Ordered Molecular Assemblies. *Nat. Mater.* **2008**, *7* (4), 326–332. https://doi.org/10.1038/nmat2119.

(45) Heimel, G.; Salzmann, I.; Duhm, S.; Koch, N. Design of Organic Semiconductors from Molecular Electrostatics. *Chem. Mater.* **2010**, *23* (3), 359–377. https://doi.org/10.1021/cm1021257.

(46) Wegner, B.; Grubert, L.; Dennis, C.; Opitz, A.; Röttger, A.; Zhang, Y.; Barlow, S.; Marder, S. R.; Hecht, S.; Müllen, K.; Koch, N. Predicting the Yield of Ion Pair Formation in Molecular Electrical Doping: Redox-Potentials versus Ionization Energy/Electron Affinity. *J. Mater. Chem. C* **2019**, *7* (44), 13839–13848. https://doi.org/10.1039/C9TC04500G.

(47) Dürr, A. C. C.; Nickel, B.; Sharma, V.; Täffner, U.; Dosch, H. Observation of Competing Modes in the Growth of Diindenoperylene on SiO2. *Thin Solid Films* **2006**, *503* (1–2), 127–132. https://doi.org/10.1016/j.tsf.2005.11.115.

(48) Yang, S. Y.; Shin, K.; Park, C. E. The Effect of Gate-Dielectric Surface Energy on Pentacene Morphology and Organic Field-Effect Transistor Characteristics. *Adv. Funct. Mater.* **2005**, *15* (11), 1806–1814. https://doi.org/10.1002/adfm.200400486.

(49) Yamada, T.; Hasegawa, T.; Hiraoka, M.; Matsui, H.; Tokura, Y.; Saito, G. Control of Film Morphology and Its Effects on Subthreshold Characteristics in Dibenzotetrathiafulvalene Organic Thin-Film Transistors. *Appl. Phys. Lett.* **2008**, *92* (23), 1–4. https://doi.org/10.1063/1.2940593.

(50) Dürr, A. C.; Schreiber, F.; Münch, M.; Karl, N.; Krause, B.; Kruppa, V.; Dosch, H. High Structural Order in Thin Films of the Organic Semiconductor Diindenoperylene. *Appl. Phys. Lett.* **2002**, *81* (12), 2276–2278. https://doi.org/10.1063/1.1508436.

(51) Scholz, R.; Gisslén, L.; Schuster, B.-E.; Casu, M. B.; Chassé, T.; Heinemeyer, U.; Schreiber, F. Resonant Raman Spectra of Diindenoperylene Thin Films. *J. Chem. Phys.* **2011**, *134* (1), 014504. https://doi.org/10.1063/1.3514709.

(52) Cheng, H. L.; Mai, Y. S.; Chou, W. Y.; Chang, L. R.; Liang, X. W. Thickness-Dependent Structural Evolutions and Growth Models in Relation to Carrier Transport Properties in Polycrystalline Pentacene Thin Films. *Adv. Funct. Mater.* **2007**, *17* (17), 3639–3649. https://doi.org/10.1002/adfm.200700207.

(53) Girlando, A.; Pecile, C.; Painelli, A. Vibrational Spectroscopy of Mixed Stack Organic Semiconductors: Comparison with Segregated Stack Systems. *Le J. Phys. Colloq.* **1983**, *44* (C3), C3-1547-C3-1550. https://doi.org/10.1051/jphyscol/1983060.

(54) Tanaka, M.; Shimizu, M.; Saito, Y.; Tanaka, J. Raman Spectra of Radical Ion DBTTF Complexes; Relation between Raman Frequency and Formal Charge. *Chem. Phys. Lett.* **1986**, *125* (5–6), 594–596. https://doi.org/10.1016/0009-2614(86)87106-8.

(55) King, R. B. Organosulfur Derivatives of the Metal Carbonyls. III. The Reaction between Molybdenum Hexacarbonyl and Bis-(Trifluoromethyl)-Dithietene. *Inorg. Chem.* **1963**, *2* (3), 641–642. https://doi.org/10.1021/ic50007a056.
(56) Davison, A.; Edelstein, N.; Holm, R. H.; Maki, A. H. Synthetic and Electron Spin Resonance Studies of Six-Coordinate Complexes Related by Electron-Transfer Reactions. *J. Am. Chem. Soc.* **1964**, *86* (14), 2799–2805. https://doi.org/10.1021/ja01068a010.
(57) Greiner, D.; Hinrichs, V.; Wiesner, S.; Ludwig, W.; Fostiropoulos, K.; Keiper, D.; Baumann, P. K.; Meyer, N.; Heuken, M.; Rusu, M.; Lux-Steiner, M. C. Optical Constants of Diindenoperylene in the Dependence of Preparation Temperature and Pressure. *Thin Solid Films* **2013**, *534*, 255–259. https://doi.org/10.1016/j.tsf.2013.03.014.
(58) Lee, J.; Kim, S. S.; Kim, K.; Kim, J. H.; Im, S. Correlation between Photoelectric and Optical Absorption Spectra of Thermally Evaporated Pentacene Films. *Appl. Phys. Lett.* **2004**, *84* (10), 1701–1703. https://doi.org/10.1063/1.1668328.
(59) Wang, K.; McConnachie, J. M.; Stiefel, E. I. Syntheses of Metal Dithiolene Complexes from Thiometalates by Induced Internal Redox Reactions. *Inorg. Chem.* **1999**, *38* (19), 4334–4341. https://doi.org/10.1021/ic990204k.
(60) Kireev, S. V; Shnyrev, S. L. Study of Molecular Iodine, Iodate Ions, Iodide Ions, and Triiodide Ions Solutions Absorption in the UV and Visible Light Spectral Bands. *Laser Phys.* **2015**, *25* (7), 075602. https://doi.org/10.1088/1054-660X/25/7/075602.
(61) Fontana, I.; Lauria, A.; Spinolo, G. Optical Absorption Spectra of Fe2+ and Fe3+ in Aqueous Solutions and Hydrated Crystals. *Phys. status solidi b* **2007**, *244* (12), 4669–4677. https://doi.org/10.1002/pssb.200743103.
(62) Özen, G.; Demirata, B. Energy Transfer Characteristics of the Hydrogen Peroxide Induced Ce3+–Ce4+ Mixture. *Spectrochim. Acta Part A Mol. Biomol. Spectrosc.* **2000**, *56* (9), 1795–1800. https://doi.org/10.1016/S1386-1425(00)00237-7.
(63) Bamwenda, G. R.; Uesigi, T.; Abe, Y.; Sayama, K.; Arakawa, H. The Photocatalytic Oxidation of Water to O2 over Pure CeO2, WO3, and TiO2 Using Fe3+ and Ce4+ as Electron Acceptors. *Appl. Catal. A Gen.* **2001**, *205* (1–2), 117–128. https://doi.org/10.1016/S0926-860X(00)00549-4.
(64) Szczepanski, J.; Wehlburg, C.; Vala, M. Vibrational and Electronic Spectra of Matrix-Isolated Pentacene Cations and Anions. *Chem. Phys. Lett.* **1995**, *232* (3), 221–228. https://doi.org/10.1016/0009-2614(94)01340-2.
(65) Salzmann, I.; Heimel, G.; Duhm, S.; Oehzelt, M.; Pingel, P.; George, B. M.; Schnegg, A.; Lips, K.; Blum, R.-P.; Vollmer, A.; Koch, N. Intermolecular Hybridization Governs Molecular Electrical Doping. *Phys. Rev. Lett.* **2012**, *108* (3), 035502. https://doi.org/10.1103/PhysRevLett.108.035502.
(66) Konarev, D. V.; Zubavichus, Y. V.; Slovokhotov, Y. L.; Shul'ga, Y. M.; Semkin, V. N.; Drichko, N. V.; Lyubovskaya, R. N. New Complexes of Fullerenes C60 and C70 with Organic Donor DBTTF: Synthesis, Some Properties and Crystal Structure of DBTTF·C60·C6H6 (DBTTF=dibenzotetrathiafulvalene). *Synth. Met.* **1998**, *92* (1), 1–6. https://doi.org/10.1016/S0379-6779(98)80000-3.
(67) Konarev, D. V.; Lyubovskaya, R. N.; Drichko, N. V.; Semkin, V. N.; Graja, A. Charge Transfer in Complexes of C60 and C70 in Solutions and Solid State. *Russ. Chem. Bull.* **1999**, *48* (3), 474–479. https://doi.org/10.1007/BF02496164.
(68) Konarev, D. V.; Lyubovskaya, R. N. Donor–Acceptor Complexes and Radical Ionic Salts Based on Fullerenes. *Russ. Chem. Rev.* **1999**, *68* (1), 19–38. https://doi.org/10.1070/RC1999v068n01ABEH000460.
(69) Tietze, M. L.; Benduhn, J.; Pahner, P.; Nell, B.; Schwarze, M.; Kleemann, H.; Krammer, M.; Zojer, K.; Vandewal, K.; Leo, K. Elementary Steps in Electrical Doping of Organic Semiconductors. *Nat. Commun.* **2018**, *9* (1), 1182. https://doi.org/10.1038/s41467-018-

03302-z.
(70) Nanova, D.; Beck, S.; Alt, M.; Glaser, T.; Pucci, A.; Schultheiß, K.; Dieterle, L.; Schröder, R. R.; Pflaum, J.; Kowalsky, W.; Kroeger, M. Phase Separation in Ternary Charge-Transfer-Complexes. *Appl. Phys. A Mater. Sci. Process.* **2013**, *112* (4), 1019–1025. https://doi.org/10.1007/s00339-012-7469-2.

TOC Graphic

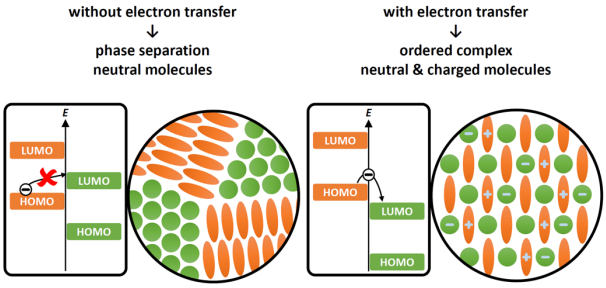
without electron transfer
↓
phase separation
neutral molecules
with electron transfer
↓
ordered complex
neutral & charged molecules
E
LUMO
HOMO
LUMO
HOMO
E
LUMO
HOMO
LUMO
HOMO